Chapter 7

The *hybrid* cone jet algorithm and the QCD systematics

A variation of the DURHAM jet algorithm is presented in this chapter, as a tool to reduce the sensitivity of the M_{W} analysis to CR, BEC and fragmentation. The first section justifies the need of the new algorithm by showing the expected values of the QCD systematics with the standard DURHAM analysis. The new *hybrid cone* algorithm is described in Section 7.2, and the optimisation and performance of the new algorithm is discussed afterwards. Section 7.6 describes a method to study CR effects on $\mathrm{W}^+\mathrm{W}^-$ events by the comparison of the results of the standard and the new cone analysis.

7.1 Estimation of the QCD systematics using the standard analysis

The estimation of the effect on the M_{W} measurement is performed using the same method for fragmentation, BEC and CR. The principle consists in applying the whole analysis on samples of MC that have been generated using different models of the effects, and comparing the measured values of M_{W}.

For the case of BEC and CR, the comparison is made between the mass measured for samples with and without the model implemented. For fragmentation, the shift is taken between samples *hadronised* with JETSET, HERWIG and ARIADNE. Such mass shifts can be used to optimise the analysis. However, for the estimation of the systematic uncertainty, a comparison between data and MC of the fragmentation-related variables would be more

correct. There is the prospect to proceed in that way for the final publication of the mass measurement of the LEP experiments.

The determination of mass biases due to BE, CR and different fragmentation models can be done in the ALEPH computing environment with a high precision and a reasonable amount of computing time with the help of the KINAGAIN interface. It allows to produce MC samples with different fragmentation options, while sharing identical events at the hard process level. This reduces the statistical error of the comparison, by minimising fluctuations between samples.

The set of options available in KINAGAIN span the three hadronisation models, but also the possibility of including BEC (BE_3 model, allowing to switch separately intra-W and inter-W correlations) and CR effects (SK1, SK2', SK2, GAL, HWCR, AR1 and AR2). In all the models that share the JETSET perturbative cascade, this stage is also forced to be identical, further improving the statistical power of the checks.

Table 7.1 summarises the mass bias (ΔM_W) obtained for every model. Also the amount of MC events available in each case and at every $\sqrt{s}$ is shown. The mass shifts in the table are obtained by averaging the shifts at each $\sqrt{s}$, weighted with the corresponding luminosity. The statistical uncertainty of the observed mass shift is computed by splitting the available MC in subsamples of 5,000 MC events.

For the alternative hadronisation models (ARIADNE and HERWIG), ΔM_W is taken with respect to a sample of JETSET with the same events at the hard process level. For all CR models based on JETSET, the difference is taken to a same sample with identical hard process events and parton shower but with standard JETSET hadronisation. In the particular case of SK1, the shift is computed for the cases with $P_{reco} = 100\%$ and with $\kappa_I = 2.13$. The second case will be the choice used for the computation of systematic uncertainties, as justified in Section 3.3.2. For HWCR and AR2, the difference is taken to a sample of same events at the hard process level produced with the same generator without CR implemented. For BE_3, the difference is taken between the implementations of BE between all pions and only intra-W.

The shifts in Table 7.1 are used for the estimation of QCD-related systematic uncertainties on M_{W}. As already mentioned, extreme values of SK1 are ruled out by the particle flow analysis (see Section 3.3.2), and the value of ΔM_W used for the estimation is that corresponding to $\kappa_I = 2.13$. With this value of the parameter, the SK1 model gives the largest CR bias among the models considered. Note that ΔM_W is very small for the

Effect	Model	MC available at	Total events (millions)	Mass shift (MeV)
Fragmentation	HERWIG	189 & 207 GeV	6	11 ± 3
	ARIADNE	189 & 207 GeV	6	3 ± 3
Colour Reconnection	SK1, 100%	all energies	4	420 ± 3
	SK1, $\kappa_I = 2.13$	all energies	4	115 ± 2
	SK2'	189 GeV	0.5	-11 ± 7
	SK2	189 GeV	0.5	-11 ± 7
	HWCR	all energies	4	38 ± 3
	GAL	all energies	1	42 ± 6
	AR1	207 GeV	0.5	0 ± 8
	AR2	all energies	1	72 ± 3
BEC	BE_3^{all}	all energies	2	-40 ± 5

Table 7.1: Mass biases due to QCD-related effects. For CR models based on JETSET and for standard HERWIG and ARIADNE, ΔM_W is taken from a standard JETSET sample. For AR2 and HWCR, ΔM_W is taken from the corresponding fragmentation model with no CR. For BEC, the shift corresponds to the difference between the model BE_3 between all pions and only intra-W. The shifts are obtained averaging MC at all available energies, weighted with the corresponding luminosity.

SK2' and SK2 models, as well as for AR1 .

For the case of BEC, only the LUBOEI local model is implemented in the ALEPH computing environment. Some studies have estimated the effect on M_{W} predicted by several global models [44, 112]. The studies do not include detector simulation, hence they only test BEC effects trough jet clustering. The mass biases obtained are always smaller than 20 MeV. For the case of the Lund weighting model, the maximum bias observed is +12 MeV [113].

The centre-of-mass energy dependence of the shift corresponding to each model has been studied. The only significant energy dependence has been found for SK1 . Fig. 7.1 shows the mass shift as a function of $\sqrt{s}$ for that model, with 100% of events reconnected and for $\kappa_I = 2.13$.

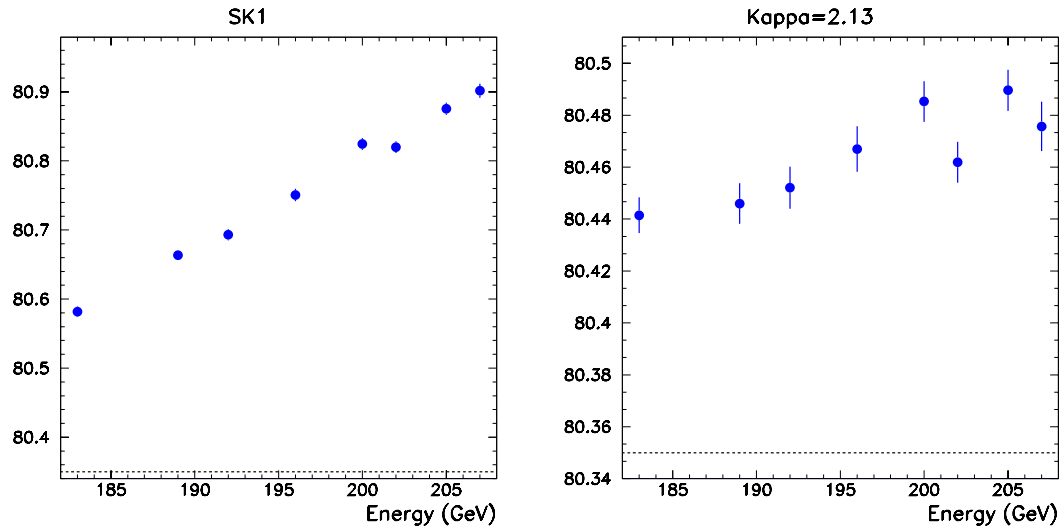

Figure 7.1: Energy dependence of the mass shift due to `SK1` , for 100% of events reconnected (left) and for $\kappa_I = 2.13$ (right).

7.2 The *hybrid* cone algorithm

The biases on M_{W} predicted by the different models indicate that the CR systematic is by far the most important in the case of the hadronic channel (see next chapter for comparison with the rest of the uncertainties). Its relevance is enhanced in the LEP-wide combination, as the CR uncertainty is assumed to be correlated between all the experiments. That has motivated a re-design of the M_{W} analysis that takes into account QCD systematics and not only the statistical performance. In particular, new jet-clustering algorithms have been considered.

The differences between events fragmented independently and events that are colour-reconnected are *a priori* expected to arise in some particular regions of the phase space. As the cores of the jets are far away in momentum and their production points are far in space-time, they could be mostly unaffected. On the contrary, the phase space in the inter-jet regions could show maximal differences between reconnected and non-reconnected configurations, in terms of local multiplicity or energy spectrum. That is confirmed in most of the models by the results of the particle flow analysis. A similar argumentation can be made about BEC effects.

In the standard analysis based in the `DURHAM` algorithm, all the energy flows are clus-

tered in one of the four jets, and all of them contribute with the same weight in the computation of the jet direction and energy. This is a common feature of the DURHAM/JADE family of algorithms. Nevertheless, there is another group of jet algorithms, widely used in hadronic colliders, where not all the energy flows -or calorimeter towers- are used. The so-called cone algorithms [114] make use only of the particles within a given angle around the jet core to compute the energy and momentum (this is technically done by an iterative process).

Cone algorithms are the most appropriate in hadronic environments, where lots of spurious activity is present in the calorimeters due to underlying QCD events. Applying the angular cut removes information, but that is compensated by the decrease of noise.

The problem is similar in the case of hadronic W^+W^- events: the *purer* information is expected to lay in the core of the jet. Removing particles in the outermost part deteriorates the statistical performance of the jet reconstruction, but this could be compensated with the reduction of sensitivity to CR, BEC and fragmentation effects. This motivated the use of a cone algorithm in the context of hadronic W^+W^- events at ALEPH.

However, a modified version of the cone algorithm has been proved to give a better performance than the standard implementation. Some studies that have compared the set of reconstructed DURHAM jets in the colour reconnected and standard versions of the same MC events conclude that the main difference between the two sets of jets is the jet angle, and not the jet energies. When particles are *moved* to the inter-jet region by CR, the jet angle is modified, but jets are still forced to conserve energy. Hence, while the use of a cone algorithm was appealing to reduce the sensitivity to CR of the jet angles, the energy measurement was only expected to be statistically degraded.

In addition, one would want the new algorithm to be a minimal deviation from the standard DURHAM one. This would mean that the sources of systematic uncertainties would be common. In addition, a large correlation between the CR-insensitive algorithm and DURHAM allows to measure CR effects, as it will be shown in Section 7.6.

The *hybrid cone* algorithm proposed in next section fulfils the requirement of being a minimal deviation of the DURHAM algorithm. In addition, the preliminary studies based on statistic and systematic uncertainties favoured the new algorithm instead of the classic cone algorithms used in hadronic colliders.

7.2.1 Definition of the hybrid cone algorithm

The denomination of *hybrid* comes from the fact that the collection of DURHAM jets are taken as a starting point for the determination of the cone jets. The DURHAM jets are always four by construction in the case of W^+W^- events. Every DURHAM jet is taken separately, and the following algorithm is applied within each of them:

- The DURHAM jet axis is taken as the cone *seed*.
- A cone of a given opening angle (R) is defined around the seed.
- The three-momenta of all the energy flow within the cone (and belonging to the original DURHAM jet) are added.
- The vector obtained by the sum of the three-momenta is used as the seed of a new cone.
- The process is iterated until a stable situation is reached, i.e., until the sum of the momenta of all energy flows within the cone coincides with the cone axis. Then the momentum four-vector of particles within the cone is taken: $(E_{inside}, \vec{p}_{inside})$. In general (but not always), the vector is different from that of the original DURHAM jet.
- The cone jet four-momentum is formed. The energy is directly taken from the DURHAM jet:

  $$E_{cone} = E_{Durham} \tag{7.1}$$

  The direction is given by particles inside the cone, but the three-momentum is rescaled in the following way:

  $$\vec{p}_{cone} = \vec{p}_{inside} \cdot \left| \frac{E_{Durham}}{E_{inside}} \right| \tag{7.2}$$

  This makes the velocity of the cone jet equal to that of the particles inside the cone. In conclusion, the jet velocities (not allowed to vary by the kinematic fit) and the jet directions (for which very small variations are allowed) are computed using the particles within the cone only.

Some remarks on the cone algorithm are:

- The association between energy flows and jets is not modified with respect to that of the DURHAM jets.

- In general, not all the energy flows are used for the computation of the jet direction and velocity.

- In the limit of large opening angle R, all energy flows are included in the cone and the standard DURHAM jets are recovered.

- R can be adjusted to optimise the balance of statistical and systematic uncertainties.

Fig. 7.2 shows the fraction of the energy of the original DURHAM jet that is carried by the particles clustered in a cone jet, as a function of R. Hadronic W^+W^- events (from JETSET MC and from all available data for $\sqrt{s} > 189\,\text{GeV}$) are used. Note that for $R > 1.5\,\text{rad}$, all the particles from the original DURHAM jet are contained, and the cone and DURHAM jets coincide. For cones with $R =\sim 0.5\,\text{rad}$, the particles left out of the cone jet carry almost 10% of the DURHAM jet energy.

As explained in Section 3.1, fragmentation effects can bias the M_W measurement through discrepancies between data and MC in the description of jet overlap regions. The use of a cone algorithm can reduce the bias, because particles in jet overlaps are far from the jet axis and some of them will be dismissed. This is illustrated in Fig. 7.3, which shows the angular distribution of energy of particles belonging to the other jets around the axis of a given jet. From the comparison of Figures 7.2 and 7.3, it can be concluded that the cone algorithm should reduce the sensitivity to fragmentation effects through jet overlaps. Another conclusion from Fig. 7.3 is that, for a given jet, the jet from the decay of the *other* W boson is in average closer than that from the same W decay.

Detailed studies on the comparison of the performance of the cone algorithm between data and MC are described in section 8.6.

7.2.2 The cone analysis

In order to perform the M_W measurement using the cone jet algorithm, some of the steps of the selection/reconstruction chain have been re-optimised. The new analysis based on the hybrid cone algorithm will be referred below as the *cone analysis*, in contrast with the DURHAM-based *standard analysis*. To optimise the performance of the analysis, it has been performed completely using eight different values of R: 1.25, 1.0, 0.9, 0.8, 0.75, 0.7, 0.6, 0.5 and 0.4 rad. Some comments on the selection and reconstruction processes of the cone analysis follow.

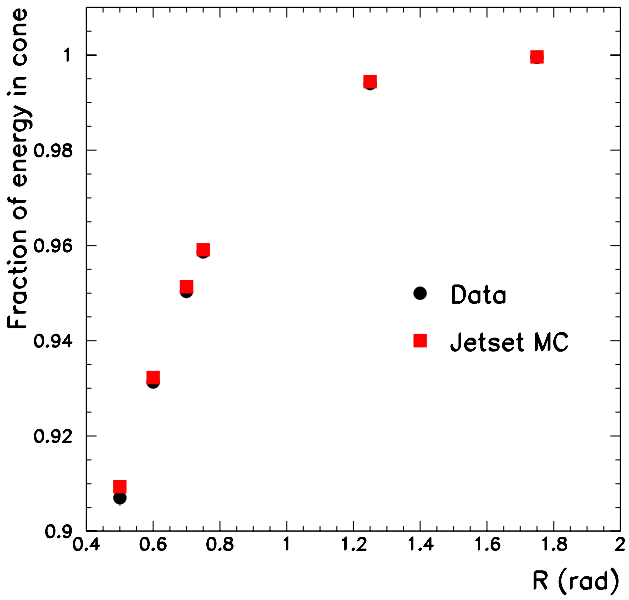

Figure 7.2: Ratio between the energy carried by the particles clustered by the cone algorithm and that of the original DURHAM jet, for several values of the opening angle of the cone R. Results are shown for events selected as hadronic W^+W^- , for JETSET MC and all the data collected for $\sqrt{s} > 189\,\text{GeV}$.

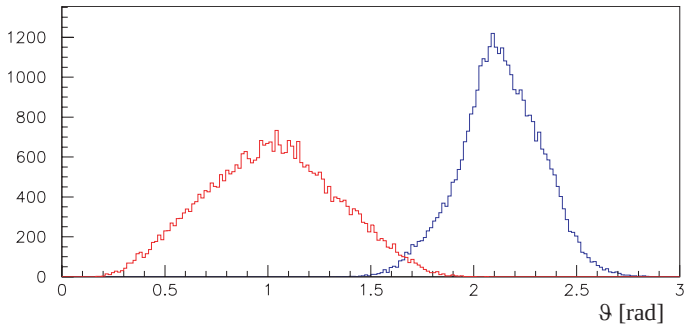

Figure 7.3: Angular distribution of energy from particles belonging to other jets around a jet axis (the angle is given in radians). The dotted histogram (left) corresponds to particles from the closest jet coming from a different W. The solid histogram (right) corresponds to the jet from to the same W. Hadronic W^+W^- MC events generated with JETSET are used.

- **Selection:** The preselection and NN selection are kept identical to the standard analysis (DURHAM jets are used as input of the NN), in order to minimise statistical

uncertainties in the comparison of the results. Only the effect of the mass window cuts makes a difference between the selections of the standard and the cone analysis. Table 7.2 shows the final efficiency and purity of the selection for the standard analysis and the cone analysis at several values of R, at 189 GeV.

Analysis	Efficiency (%)	Purity (%)
Standard	80.2	85.8
Cone, $R = 1.0$	79.1	84.3
Cone, $R = 0.75$	77.8	84.3
Cone, $R = 0.5$	76.7	84.2

Table 7.2: Efficiencies and purities of the selections for standard and cone analysis at $\sqrt{s}$ = 189 GeV, as computed from a sample of one million MC events. Differences are due only to the window cut.

- **Kinematic fit:** The kinematic fit is performed in exactly the same way for cone and standard jets. A different parameterisation of the energy resolution is used for each value of the R parameter.

- **Jet energy corrections:** As the energy of the jets is the same as for `DURHAM`, minimal deviations are expected, only through the angular dependence of the corrections. However, a dedicated set of values has been computed for the cone algorithm, as shown in Fig. 7.4. The corrections corresponding to standard jets are also plotted in the figure with their statistical error, showing that the relative differences are small.

- **Jet pairing:** The algorithm used is the same as for the standard analysis.

The linearity of the measurement of M_{W} using the cone analysis has been checked in the same way as described in Section 6.3.1 for the standard analysis. MC samples of 200K events generated with several values of M_{W} have been fitted, and the dependence between the fitted and the generated masses has been found to be compatible with a straight line, with no offset and unitary slope, for all the values of R considered. This is shown in Fig. 7.5 for two values of R.

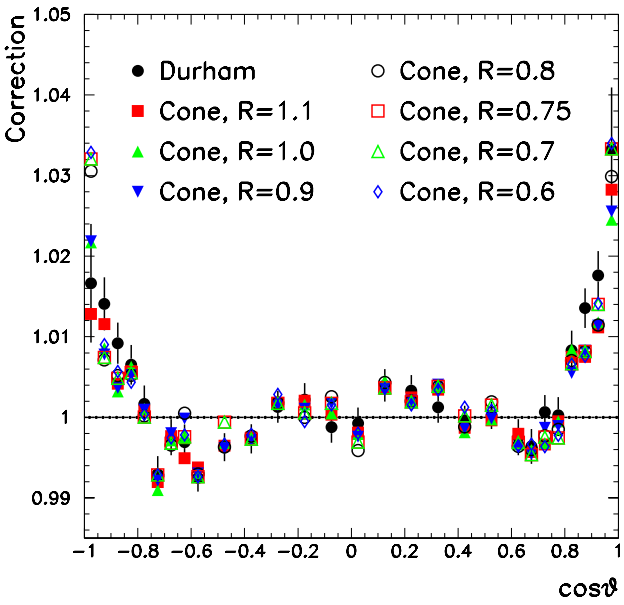

Figure 7.4: Jet corrections derived from 1998 Z data and MC as a function of jet polar angle, for several values of R.

7.3 Statistical performance of the cone algorithm

As the cone analysis dismisses part of the information of the events, a degradation of the statistical precision of the mass measurement is expected. Fig. 7.6 shows the degradation as a function of R. A total of 2.5 millions of MC events generated at $\sqrt{s} = 189$ and 207 GeV have been used for the computation.

In Fig. 7.6, as well as in the rest of plots that follow in this chapter, the point labelled $R = 2.0$ rad corresponds in fact to the result obtained with standard `DURHAM` . It is plotted at $R = 2.0$ rad in order to allow a simple visualisation.

The statistical degradation of the cone analysis is directly related to the information carried by the particles left outside the cone. This can be seen in Fig. 7.7, that shows the statistical uncertainty as a function of the average energy carried by the energy flows left out of the cone.

Table 7.3 shows the results of the mass fits for each $\sqrt{s}$, for the standard analysis and for the cone analysis with three values of R (27 MeV have been added to account for the

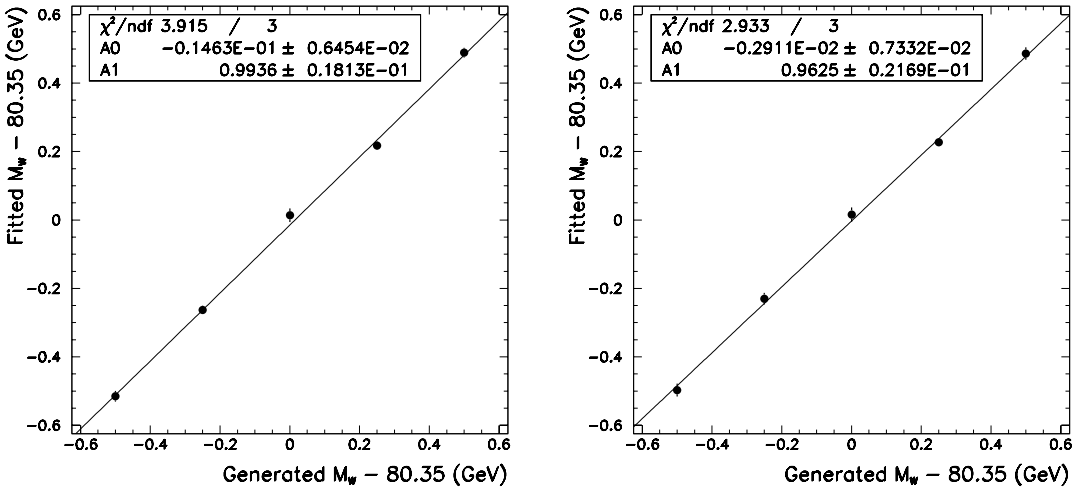

Figure 7.5: The fitted M_{W} versus the generated M_{W}, using the cone analysis. The plot on the left corresponds to $R = 1.0$ rad, and the one on the right to $R = 0.5$ rad. The result of straight line fits to the points are shown as solid lines and the values of the offset (A0) and the slope (A1) are given in the plots, together with the χ^2 of the fits. The fits are compatible with straight lines with no offset and slope equal to unity.

difference between running and fixed width schemes, as justified in Section 2.3).

	Fitted mass (GeV)			
$\sqrt{s}$	Standard	$R = 1$ rad	$R = 0.75$ rad	$R = 0.5$ rad
183	80.499 ± 0.185	80.403 ± 0.177	80.654 ± 0.202	80.646 ± 0.206
189	80.580 ± 0.106	80.590 ± 0.108	80.532 ± 0.119	80.628 ± 0.132
192	80.285 ± 0.252	80.291 ± 0.246	80.028 ± 0.270	80.440 ± 0.301
196	80.532 ± 0.147	80.569 ± 0.150	80.444 ± 0.161	80.235 ± 0.173
200	80.250 ± 0.158	80.373 ± 0.164	80.238 ± 0.182	80.273 ± 0.208
202	80.484 ± 0.241	80.535 ± 0.281	80.783 ± 0.274	80.413 ± 0.339
205	80.529 ± 0.140	80.457 ± 0.140	80.509 ± 0.159	80.523 ± 0.174
207	80.657 ± 0.118	80.544 ± 0.123	80.407 ± 0.126	80.371 ± 0.159

Table 7.3: Results of the of M_{W} from data, showing the statistical uncertainties obtained from the fit.

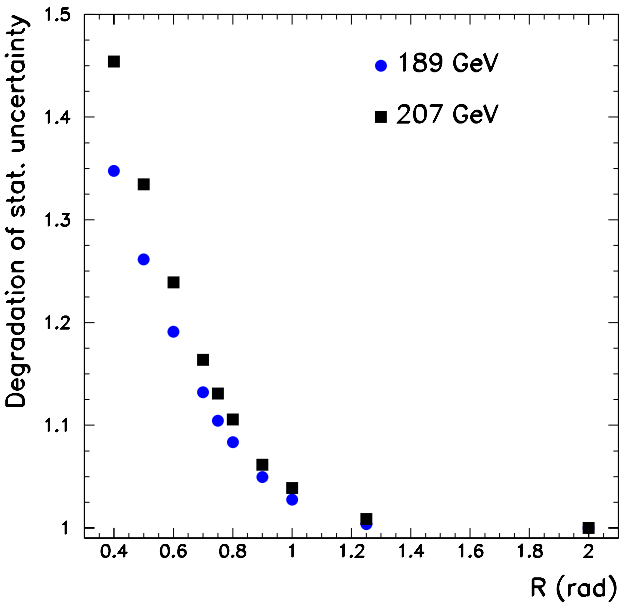

Figure 7.6: Degradation of the expected statistical uncertainty in the M_{W} measurement as a function of R. The uncertainty is computed using MC samples of 2.5M events at 189 and 207 GeV. The point at $R = 2$ rad corresponds to the standard analysis.

7.4 The QCD systematics and the cone analysis

In order to study the sensitivity of the new cone analysis to the different QCD effects, the corresponding mass shifts have been recomputed. The plots in this section show the dependence of the values of ΔM_W on R. For all of them, the standard `DURHAM` analysis is arbitrarily labelled as $R = 2.0$ rad, in order to allow a clear visualisation. The shifts and the statistical uncertainties are computed using all available MC, as described in Section 7.1.

7.4.1 Sensitivity to fragmentation

The dependence of the fragmentation-related mass shifts (`HERWIG-JETSET` and `ARIADNE-JETSET`), are shown in Fig. 7.8. Note that there is a tendency to increase ΔM_W when smaller cones are used.

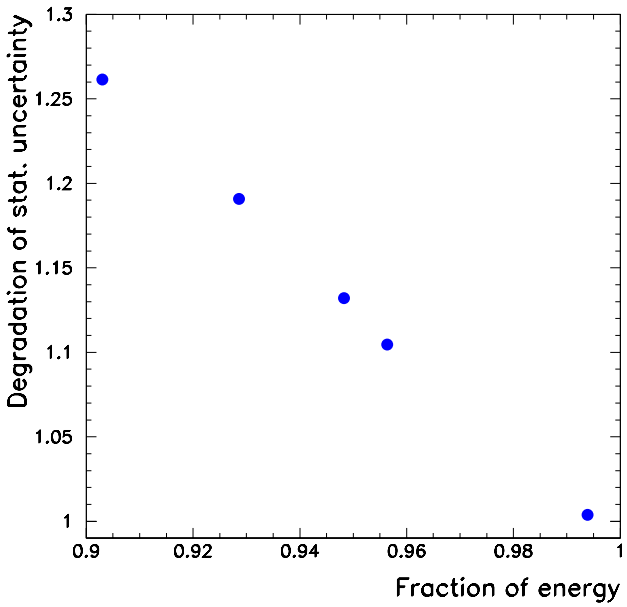

Figure 7.7: Degradation of the expected statistical uncertainty as a function of the average energy carried by the energy flows inside the cone. Each point corresponds to a different value of R.

7.4.2 Sensitivity to BEC

Fig. 7.9 shows the dependence of the BE_3 mass shift with the cone radius R. The bias is reduced from 40 MeV with the standard analysis to 22 MeV when the narrowest cones are used.

7.4.3 Sensitivity to CR

Fig. 7.10 shows the dependence of the CR mass shift for the `SK` models. For the case of `SK1`, results are shown for $P_{reco} = 100\%$ and $\kappa_I = 2.13$. It can be observed that ΔM_W decreases when narrower cones are applied, as expected. `SK2'` and `SK2` predict a relatively small ΔM_W for all the analyses.

The analogous plots for the rest of the CR models can be found in 7.11. For the case of `HWCR` and `GAL`, the mass bias is clearly reduced by the use of the cone analysis. `AR1` does not predict any significant bias, due to the fact that it only allows intra-W reconnections. Note that the fraction of the mass shift due to `AR2` that is reduced by using the cone

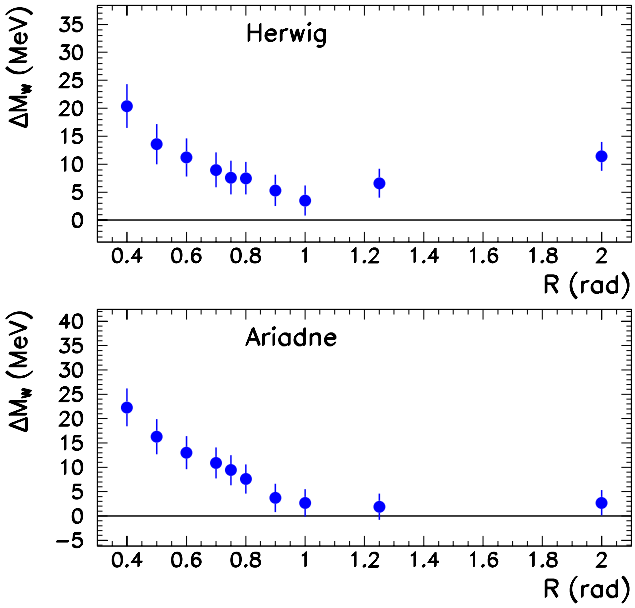

Figure 7.8: Dependence of ΔM_W due to fragmentation models on R.

algorithm is very small compared to that of other models.

7.5 Summary of the performance of the standard and cone analyses

Table 7.4 summarises the values of the mass biases due to QCD effects for the standard and cone analyses at several values of R. The statistical degradation of the measurement is also shown. In conclusion, the performance in terms of sensitivity to QCD effects improves for smaller cones, while the statistical performance degrades. The optimal value of R for the measurement of M_{W} will be the one that minimises the total uncertainty.

7.6 Study of CR effects using the cone analysis

Most of the CR models predict a more or less strong dependence of the measured M_{W} on the cone opening angle R. In particular, the difference between the cone and the standard results (ΔM_{C-S}) can be exploited to check the validity of such models. If the value of

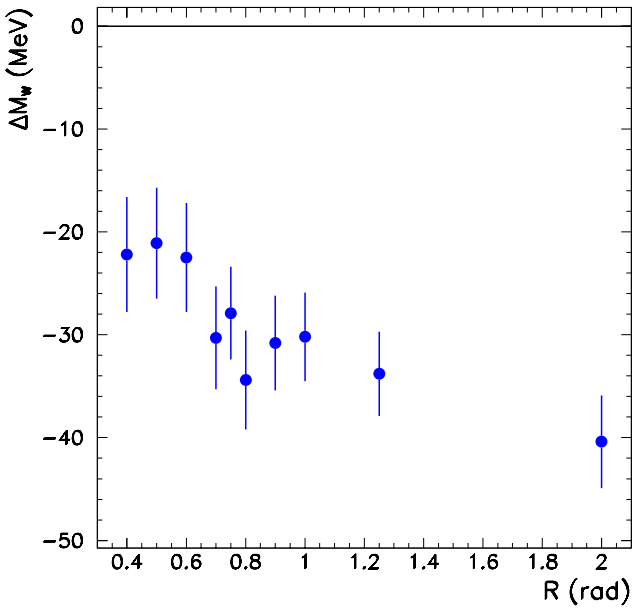

Figure 7.9: Dependence of ΔM_W due to BE_3 on R.

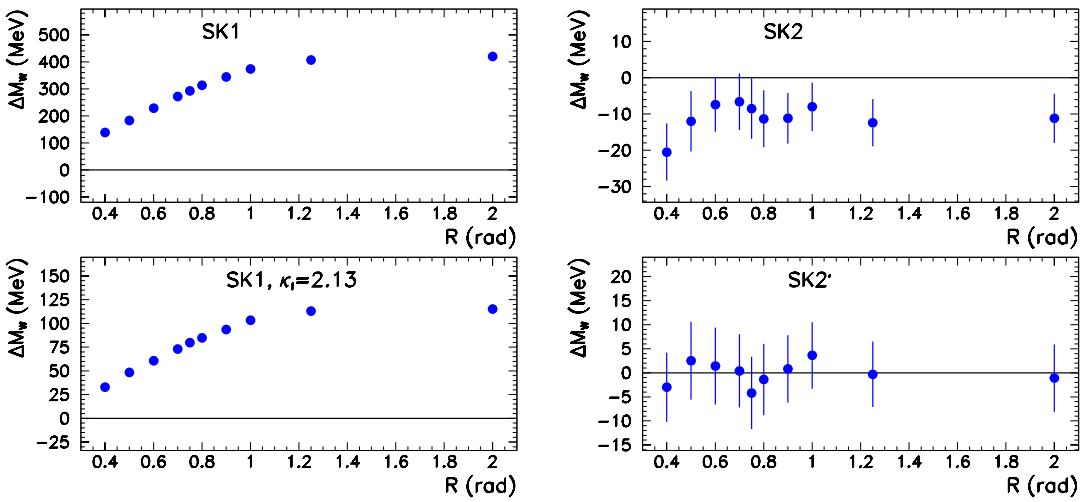

Figure 7.10: Dependence ΔM_W due to SK models on the R parameter.

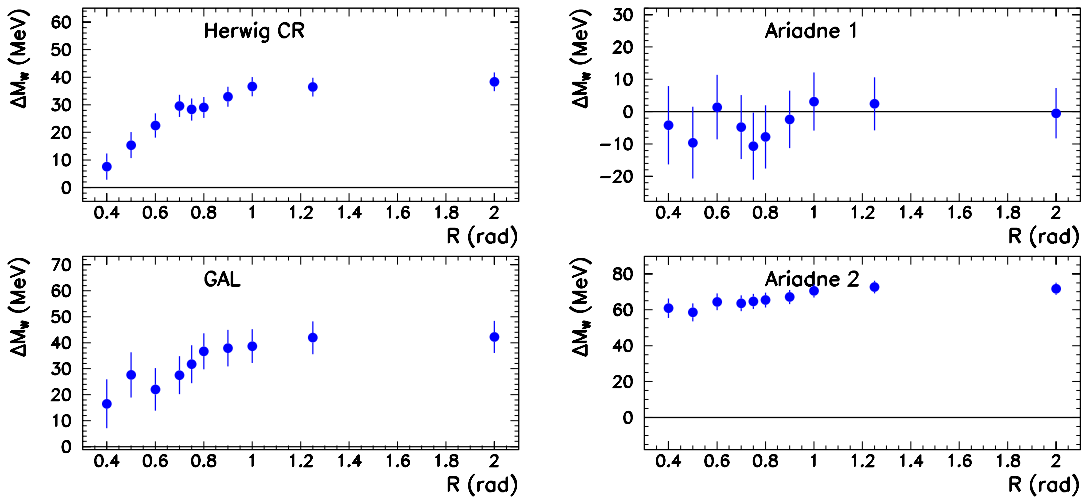

Figure 7.11: Dependence of the mass shift due to SK2', SK2, HWCR and GAL on the R parameter.

		ΔM_W (MeV)			
Effect	Model	Standard	$R = 1.0$ rad	$R = 0.75$ rad	$R = 0.5$ rad
Frag.	HERWIG	11 ± 3	3 ± 3	8 ± 3	14 ± 4
	ARIADNE	3 ± 3	3 ± 3	9 ± 3	16 ± 4
CR	SK1, 100%	420 ± 3	374 ± 3	293 ± 3	183 ± 4
	SK1, $\kappa_I = 2.13$	115 ± 17	103 ± 2	80 ± 2	48 ± 3
	SK2'	-11 ± 7	-12 ± 7	-9 ± 8	-12 ± 8
	SK2	-1 ± 7	4 ± 7	-4 ± 7	3 ± 8
	HWCR	38 ± 3	37 ± 4	28 ± 4	15 ± 5
	GAL	42 ± 7	39 ± 7	32 ± 7	28 ± 9
	AR1	0 ± 8	3 ± 9	-11 ± 10	-10 ± 11
	AR2	72 ± 3	71 ± 4	65 ± 4	56 ± 5
BEC	BE_3^{all}	-40 ± 5	-30 ± 4	-28 ± 4	-21 ± 5
Stat. degradation		0%	3.0%	10.5%	26.1%

Table 7.4: Mass biases due to QCD-related effects, for the standard analysis and the cone analysis with several values of R.

ΔM_{C-S} predicted by the model is excluded by real data results, the model should be dismissed for the computation of uncertainties on M_{W}.

To exploit the maximum of information from data and MC, a χ^2 function can be built by comparing the value of ΔM_{C-S} measured at each $\sqrt{s}$ with the prediction from each model at the given $\sqrt{s}$. The statistical error in the shift can be computed by using MC subsamples of the size of data[1].

In order to estimate the sensitivity of the method, an expected χ^2 is built by assuming null mass shifts at each $\sqrt{s}$. Table 7.5 shows the expected χ^2 for several values of R and for several CR models. Those models for which there is not MC available at each $\sqrt{s}$ (`SK2'`, `SK2` and `AR1`) are not taken into account. However, this models are not relevant for the $M_{\rm W}$ analysis, as the ΔM_W that they predict is negligible.

There is a large expected sensitivity on the comparison between `SK1` with 100% of reconnections and standard `JETSET`. On the contrary, the sensitivity to other models is smaller, as the predicted value of ΔM_{C-S} is closer to zero.

In the case of the `SK1` model, the χ^2 can be computed as a function of the κ_I parameter. The resulting expected curves under the ΔM_{C-S}=0 assumption are shown in Fig. 7.12. It can be concluded that, if systematic uncertainties are not taken into account, the most sensitive observable to CR is ΔM_{C-S} using the narrowest cone, at least within the range of R studied.

The expected χ^2 taking into account systematic uncertainties is shown in next chapter, while the observed χ^2 function is given in Chapter 9.

Model	Expected χ^2 , no systematics		
	$R = 1.0$ rad	$R = 0.75$ rad	$R = 0.5$ rad
`SK1`, $P_{reco} = 100\%$	3.3	10	18.7
`SK1`,$\kappa_I = 2.13$	0.29	0.80	1.48
`HWCR`	0.22	0.14	0.13
`GAL`	0.286	0.18	0.26
`AR2`	0.031	0.023	0.037

Table 7.5: Expected values of the χ^2 function with only statistical uncertainty taken into account, in the case of measuring a null mass shift.

[1]Technically, the uncertainty on the shift is computed using standard MC without CR implemented

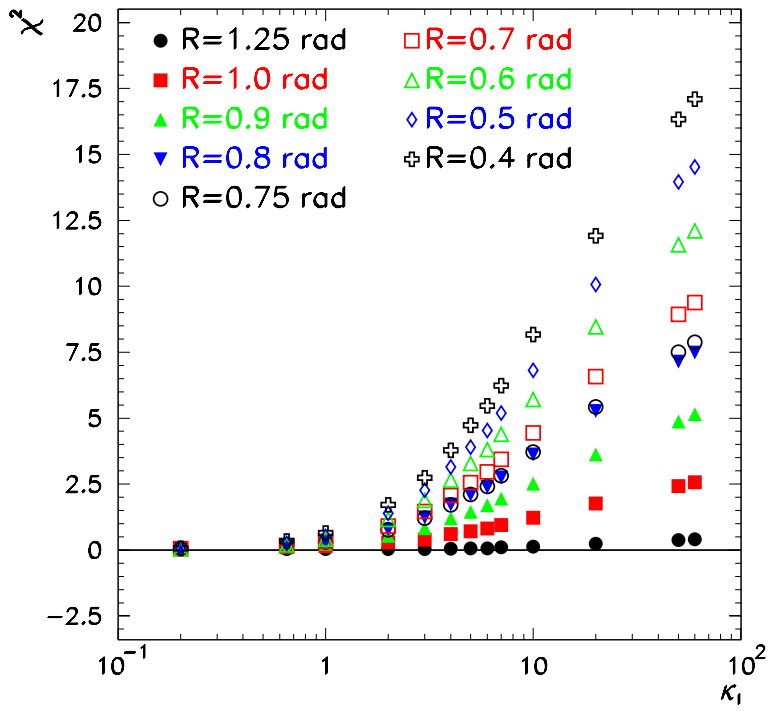

Figure 7.12: Expected values of χ^2 as a function of κ_I with only statistical uncertainty taken into account, and assuming ΔM_{C-S}=0.

Chapter 8

Systematic uncertainties

This chapter reviews the current knowledge of the systematic uncertainties in the measurement of M_{W} from the hadronic channel at ALEPH, using both the standard and cone analyses. After a list of sources common to both analyses, a study dedicated to identify new potential uncertainties in the cone analyses is reviewed. The summary of the different contributions is given in Section 8.7. discusses the systematic uncertainty in the CR studies based on the measurement of ΔM_{C-S}.

8.1 Theoretical uncertainty on the generation of the $\mathrm{W}^+\mathrm{W}^-$ hard process

`KORALW` version 1.53.2 [14] applies virtual factorisable corrections up to leading logarithm in the simulation of $\mathrm{W}^+\mathrm{W}^-$ production. In addition, it makes use of the `YFSWW3` package [15] to compute an event-by-event weight to account for the next-to-leading logarithm corrections. This weight is not applied in the MC used in this analysis. To check the effect of this missing correction, the ALEPH M_{W} analysis has been applied to MC samples with and without the weight applied. The difference is found to be of the order of 1MeV, and therefore the effect of such corrections is considered to be negligible.

The effect of the rest of missing corrections in the `KORALW`/`YFSWW3` chain is estimated in Ref. [16]. The estimation is performed at the partonic level and implementing simplified acceptances. A one-dimensional fit is applied to the W invariant mass distribution obtained from MC samples produced with several modifications of the corrections. The fitting function is obtained from a semi-analytical program (KorWan [115]). The overall

combined uncertainty is found to be less than 5 MeV. This estimate includes a factor of 2 to account conservatively for correlation effects between the masses of the W^+ and the W^-, which are fitted separately in the actual experimental procedure.

The conclusion is cross-checked by comparing the results obtained with KORALW/YFSWW3 with those obtained from an independent generator: RacoonWW [116]. The two calculations differ in most of the aspects of the implementation of all the corrections, but the difference between both results is less than 3 MeV.

A part from that, a dedicated check for ISR has been performed in ALEPH, using the whole real analysis chain. The modelling of initial state radiation in KORALW1.53.2 is performed to third order in the leading log approximation. To estimate conservatively the effect of higher order terms, $\mathcal{O}\left(\alpha^3 L^3\right)$, a sample of KORALW $\mathrm{W^+W^-}$ events are weighted by the ratio of the first and second order matrix elements squared. The difference in fitted masses for the sample with and without re-weighting is taken as an upper limit on the effect of the missing higher order terms; the difference is of the order of 5 MeV for both the standard and the cone analyses.

As the estimation of the ISR effect is included in the estimation from Ref. [16], the systematic uncertainty from the theory in the description of the $\mathrm{W^+W^-}$ process is taken as the maximum of the two approaches cited in this section. It is therefore 5 MeV for standard and cone analysis.

8.2 Background

The expected amount of background remaining in the data sample after all analysis cuts (preselection, NN selection and mass window) is about 15%. The relatively small data sample makes it difficult to compare the properties of the data and MC background events. A technique developed for previous analyses [101] uses Z data and MC, using a similar preselection to this analysis. The shape of several variables and the overall number of events are then compared. The effect of any discrepancy on the fitted M_{W} is evaluated by varying the background p.d.f. used in the reweighting step appropriately to the observed discrepancies at the Z. The estimated uncertainty on the measured M_{W} is of the order of 5 MeV [117].

The effect of the uncertainty on the overall background normalisation is tested by applying a 5% variation in the number of background events in a fitted MC sample. The

effect is found to be negligible compared to the 5 MeV from the previous test.

8.3 Monte Carlo statistics

As explained in Section 6.2.2, the finite number of MC events used to build the reference p.d.f. contributes a systematic uncertainty to the measured M_{W}. The method of calculating the uncertainty for this measurement was developed for previous measurements [101] and follows an analytical approach, taking into account that each bin in the reference probability distribution function has a different sensitivity to M_{W} as the reference distribution is reweighted.

The statistical contribution from each bin was calculated, leading to an estimate of 5 MeV for the uncertainty.

8.4 Detector effects

The technique of reweighting relies on a good MC simulation of both the underlying physics processes and the response of the ALEPH detector to these events. Therefore, the simulation of the detector has to be investigated in detail for possible discrepancies between the MC simulation and real data, and to ensure that these discrepancies are understood.

The technique used to estimate the uncertainties due to detector related effects is the same as in previous cases. The analysis is applied to a large sample of MC events, to which the effects under investigation are forcedly applied. The difference in the mass obtained with respect to the sample without the extra effect is taken as the systematic uncertainty.

8.4.1 Jet energy corrections

As explained in Section 5.2.1, corrections are applied to the energy of jets in any MC used in the analysis. The systematic uncertainty on M_{W} due to these corrections is estimated by varying randomly the bin to bin correction factors by their statistical uncertainty, which is about 0.3%. Taking the largest shift in the measured M_{W} as the systematic uncertainty, gives about 5 MeV for cone and standard analyses.

8.4.2 Calorimeter simulation

The jet corrections described in the previous section are obtained after the energy flow algorithm has been run and are applied to the jet as a whole. The individual calorimeter energy depositions can be treated in a similar way by considering differences between Z data and MC. The corrections obtained are applied to MC and the energy flow and jets recomputed to finally estimate the systematic uncertainty on M_{W}.

The simulation of the calorimeters in the MC assumes that their energy calibrations are constant with time. However, this is not the case and the calorimeters are constantly monitored to study the variations. For instance, the size of the fluctuations during 1998 were of the order of 0.4% for ECAL and 1.5% for HCAL. In addition, the jet energy corrections are determined using data from the start and end of the data taking periods hence they do not take the variations into account. To do the systematic check, the size of the fluctuations is computed in bins of azimuthal angle. A random smearing of the energy depositions in the calorimeters by these amounts is therefore applied to a MC sample and the energy flow repeated.

The shift obtained as a function of the R parameter of the cone analysis and for the Durham analysis (plotted at $R = 2.0$ rad) is shown in Fig. 8.1. The value stays below 5 MeV for all the analyses.

An independent check of the calorimeter simulation has been recently developed in ALEPH. In a dedicated MC generation of 500K events, the calorimeter was described in the GEANT program using a complete *full* simulation, instead of the usual parameterisation. For simplicity, each stack of the calorimeter was described as an average medium, namely an average of gas, lead, aluminium and plastic. The difference between the mass fitted from the full simulated sample and that from standard MC is shown in Fig. 8.2.

The systematic quoted for calorimeter simulation is taken to be 10 MeV for standard and cone analyses, coming from the maximum between the effects of energy smearing and full versus parameterised simulation. Note that some double-counting can be expected between the systematics associated to calorimeter simulation and to jet energy corrections, as jet corrections should absorb most of the discrepancies on calorimeter simulation. Taking them separately is a conservative approach.

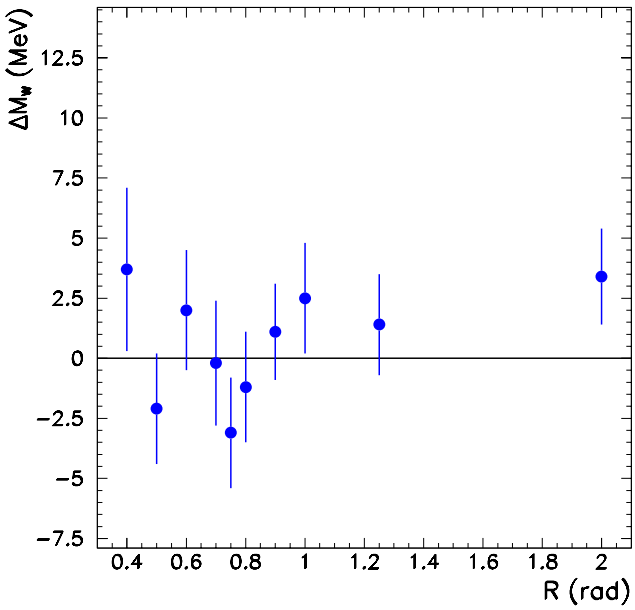

Figure 8.1: The calorimeter simulation systematic as a function of R.

8.4.3 Jet energy resolution

The jet energy resolution, $\sigma_{E_{jet}}$, is also studied using Z data and MC, in the same way as the jet energy itself. The comparison of 1998 Z data and MC jet energy resolutions is shown in Fig. 8.3 together with the comparison of the jet energies. It can be seen that the statistical uncertainty of the comparison of the resolution is greater than that for the jet energy and is at a level of about 2%, but reasonable agreement is seen over the whole angular range except for the low angle regions at $|\cos\theta| > 0.95$. There the discrepancy is as large as 10%.

In order to estimate the corresponding systematic uncertainty, the jet energies of a MC sample are randomly smeared by the appropriate amounts, depending on the jet polar angle, and the systematic uncertainty on M_{W} estimated. The result obtained for the Durham analysis in Ref. [104] was 7 MeV, and it is the same for the cone analysis as the measurement of the energy of the jet is not modified.

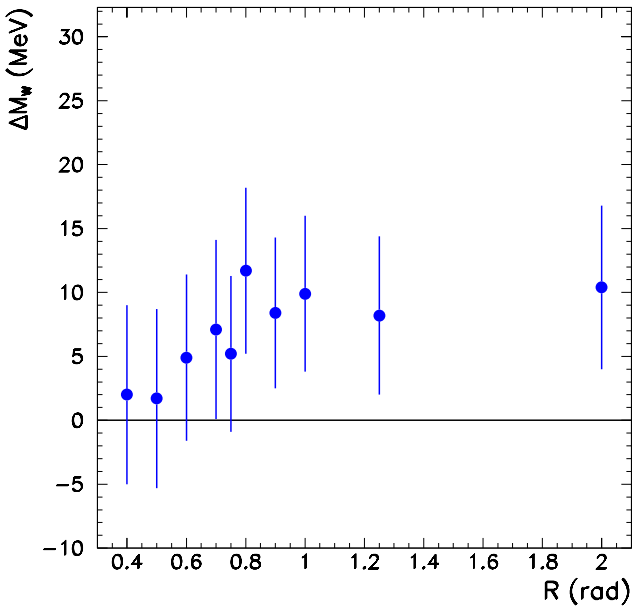

Figure 8.2: Mass shift between MC samples with full and standard simulation of the calorimeter as a function of the R.

8.4.4 Jet angular bias

The two largest components are charged particles (measured by the tracking detectors), and photons (measured by ECAL). The angular biases between the two component can be compared between data and MC to get an estimate of possible angular biases in the measurement of jet directions.

The polar angle difference between the photonic and charged particle components of jets, $\theta_{hadrons} - \theta_{photons}$, is examined using Z peak data and MC simulation. Fig. 8.4 shows this difference as a function of polar angle for the standard analysis. It can be seen that the difference is less than 2 mrad, which is the statistical sensitivity of the measurement. Studies using higher statistics from the 1994 Z data taking period show that the difference between data and MC is small for cone and standard analyses, except in the region of the overlap between the end-cap and barrel calorimeters. The result of a fit to the 1994 data is shown by the line in Fig. 8.4. The systematic uncertainty on M_{W} due to a 2 mrad angular bias is estimated to be less than 5 MeV for both analyses [104].

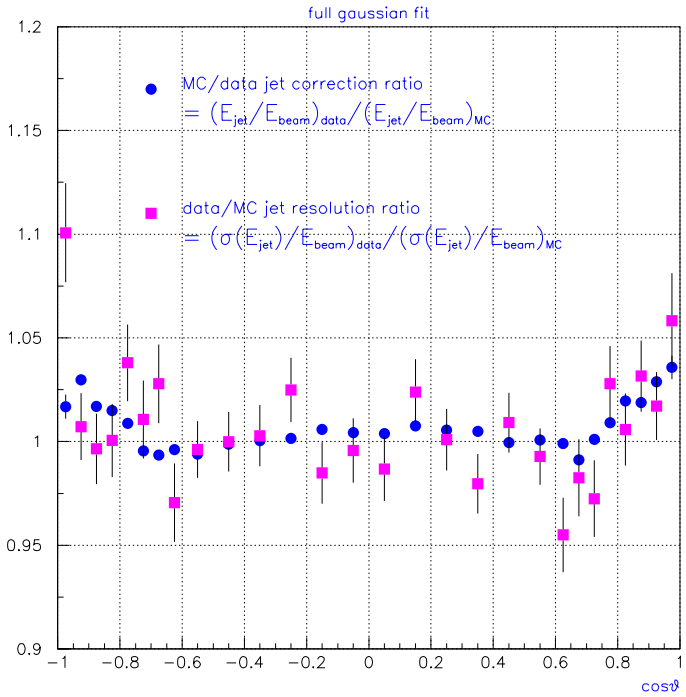

Figure 8.3: The jet energy and jet energy resolution corrections as a function of polar angle. The ratios are determined from 1998 Z peak data and MC. The largest discrepancies between data and simulation are seen in the low angle regions. Taken from [104].

8.4.5 Jet angular resolution

The fact that jets in hadronic Z decays (at $\sqrt{s} = M_Z$) should be back-to-back can be exploited to study the angular resolution of the jets. It is found that the resolution is slightly better in MC simulation than in data. A random smearing is thus introduced to the jet angles in the MC to estimate the effect on M_{W} from this discrepancy. The systematic uncertainty is found to be small, less than 5 MeV.

8.4.6 Charged particle tracking

Data from calibration runs at the Z peak are used to look for distortions in the measurements of charged particle momentum and direction at the tracking system. Small distortions are found in $Z \to \mu^+\mu^-$ and Bhabha events, where the two leptons should be exactly back-to-back. The distortions affect the measurement of both the momentum and direction of the particles. The average distortions have been measured for $|\vec{p}|$, ϕ and

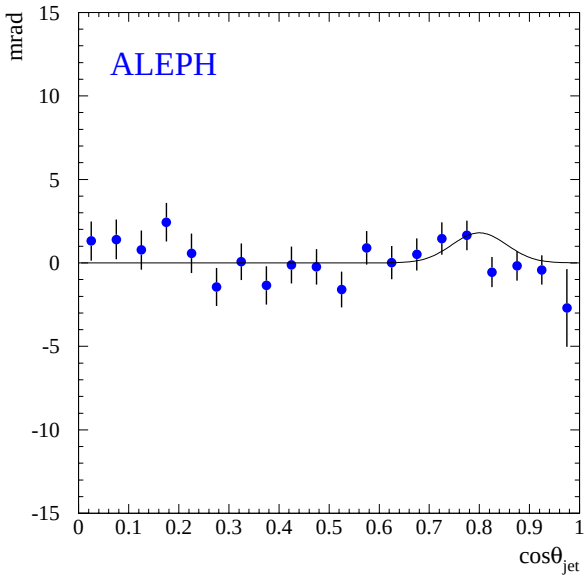

Figure 8.4: The difference of data and MC for the quantity $\theta_{hadrons} - \theta_{photons}$ as a function of jet polar angle, determined from 1998 Z data and MC. The line is a functional fit to higher statistics data from 1994, showing the discrepancy observed in the overlap region of the barrel and end-cap calorimeters.

p_z, in bins of *theta* and *phi* [118].

To estimate the corresponding systematic uncertainty on M_{W}, the distortions measured are applied to the charged particles of a MC sample. The M_{W} fitted using this sample is compared with that obtained with no correction. Results on the bias for the standard and cone analyses are shown in Fig. 8.5. The size of the systematic uncertainty quoted is 6 MeV for cone and standard analysis.

8.5 LEP energy

As explained in Section 5.2.2, the fractional uncertainty in the beam energy is expected to translate directly to a fractional uncertainty on M_{W}. This has been cross-checked by taking a sample of MC, changing the LEP energy in the kinematic fit and rescaling steps and fitting M_{W} [104].

The average uncertainty in the LEP beam energy during LEP2 was 25 MeV, that

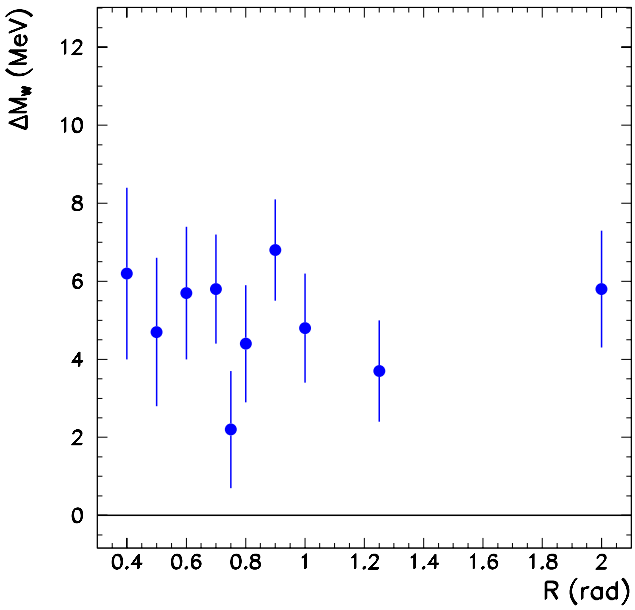

Figure 8.5: The charged particle tracking systematic as a function of R.

would translate into 17 MeV in the M_{W} measurement. However, the uncertainty of E_{beam} provided by the LEP Energy Calibration Working Group is split in four periods, corresponding to four intervals of $\sqrt{s}$: 183 GeV, 189 GeV, 192-196 GeV and $200 - 207$ GeV. Four values of the uncertainty and a 4×4 correlation matrix are provided [77]. As the correlation between measurements is lower than one, the impact of the LEP energy uncertainty in the combined measurement is reduced (see next chapter).

8.6 Dedicated studies for the cone analysis

The analysis based on the hybrid cone algorithm can have a different sensitivity to fragmentation than that based on DURHAM. As particles far from the jet axis are dismissed, it is expected to be more insensitive to the description in MC of effects like detector acceptance or jet overlaps. On the other hand, the sensitivity to the angular distribution of particles within the jet could be enhanced.

It has been shown in Subsection 7.4.1 that the mass shift between different fragmentation models is not increased when the cone algorithm is used, except for the smallest

values of R. However, a further study has been performed to check the agreement between data and MC in the angular distributions of multiplicity, energy and jet mass.

As the number of collected W^+W^- events does not allow for a significant comparison, LEP1 data has been used. A sample of 700,000 $Z \to q\bar{q}$ events was selected from data collected in 1994. The same amount of MC events produced with JETSET and HERWIG were used for the comparison. The jets were clustered with the DURHAM algorithm, and several integrated distributions as a function of the angle to the jet axis were computed.

Fig. 8.6 shows the distributions of particle multiplicity and energy, for data, JETSET and HERWIG. The bottom plots in each figure show the ratio between data and standard JETSET MC.

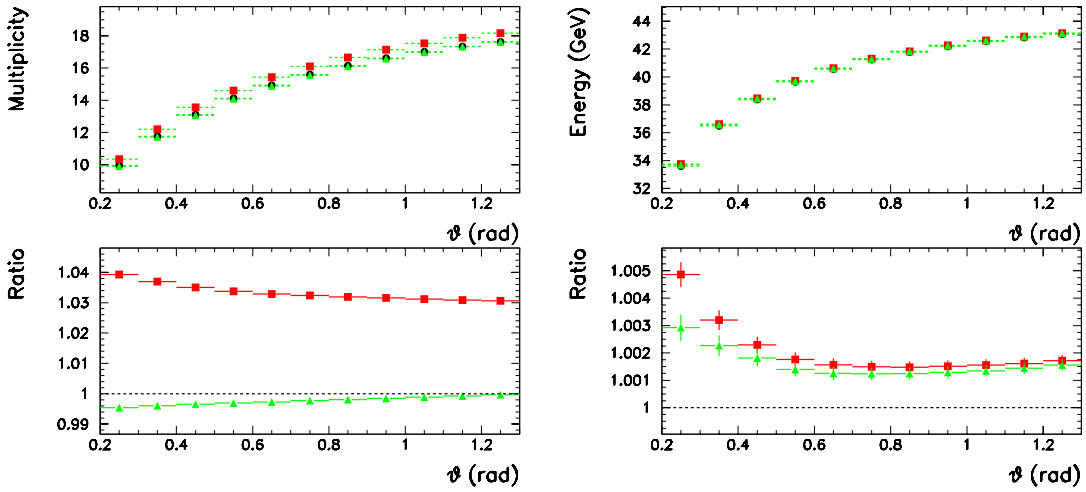

Figure 8.6: Integrated particle multiplicity (left) and jet energy (right) as a function of the angle to the jet axis, for $Z \to q\bar{q}$ from 1994 (dots), JETSET (squares) and HERWIG (triangles). Bottom plot: ratios data/JETSET (squares) and HERWIG/JETSET (triangles).

To estimate the significance of the discrepancies, the ratio HERWIG/JETSET is also shown. Note that the discrepancy data-JETSET is $\sim 3\%$ for particle multiplicity, much larger than that of HERWIG-JETSET[1]. However, the relevant distribution for the performance of the cone algorithm is integrated energy, which is in much better agreement.

The data-JETSET discrepancies in integrated energy are compatible with those from

[1]Possible explanations of the excess of multiplicity observed are currently under study. Eventual corrections can be a source of future improvement of this analysis

HERWIG-JETSET for $R > 0.5\,\mathrm{rad}$. Therefore, the effect on M_{W} should be expected to be included in the HERWIG-JETSET mass bias. As this is not true for narrower cones, results given in this thesis will be restricted to $R > 0.5\,\mathrm{rad}$, in order to avoid the presence of new sources of systematic uncertainty.

The analogous distribution for the jet mass is shown in Fig. 8.7. From the bottom plot, it can be concluded that data is in a much better agreement with HERWIG than with JETSET for this particular distribution. The discrepancies data-JETSET are comparable to that from HERWIG-JETSET in the range of R considered.

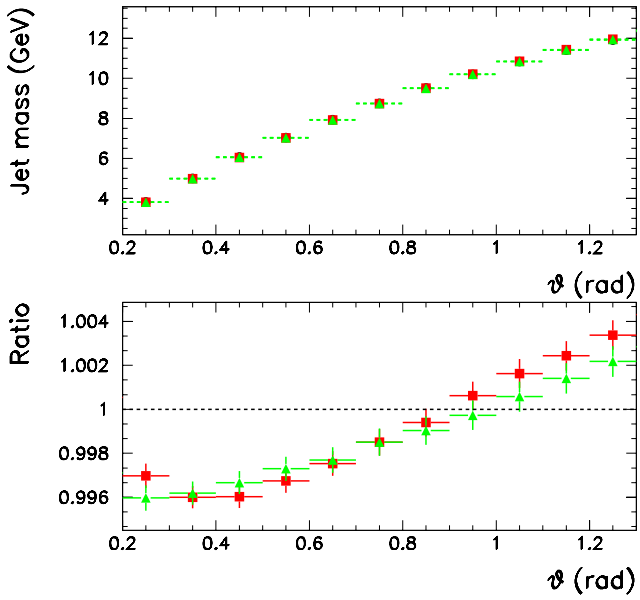

Figure 8.7: Integrated jet mass as a function of the angle to the jet axis, for $\mathrm{Z} \to \mathrm{q\bar{q}}$ data from 1994 (dots), JETSET (squares) and HERWIG (triangles). Bottom: ratios data/JETSET (squares) and HERWIG/JETSET (triangles).

The two quantities that are not allowed to vary significantly by the kinematic fit are the jet directions and the jet velocities. Therefore, the comparison between data and MC in this distributions is of special relevance. Fig. 8.8 shows the integrated distribution of velocity, using the same event samples as in the figures above. There is a good agreement between data and MC.

For the study of inter-jet angles, the topology of $\mathrm{Z} \to \mathrm{q\bar{q}}$ events is too different from

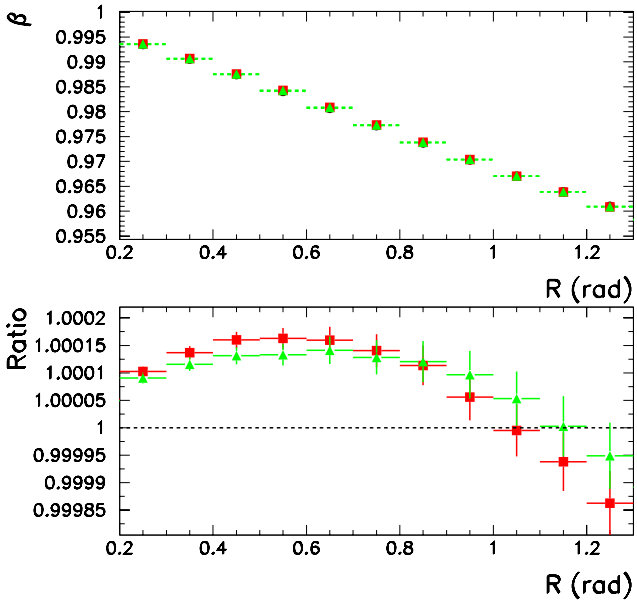

Figure 8.8: Velocity of the particles included in a cone as a function of R, for $Z \to q\bar{q}$ data from 1994 (dots), JETSET (squares) and HERWIG (triangles). Bottom: ratios data/JETSET (squares) and HERWIG/JETSET (triangles).

that of the signal to be a valid benchmark. Instead, semileptonic W^+W^- events have been used. Their topology is very similar to that of the signal, but they are a completely independent sample. In addition, semileptonic events are free from any inter-W CR effects that could distort the comparison. The results are shown in Fig. 8.9.

The conclusion from all the checks performed is that there is no evidence of new sources of systematic uncertainty in the cone analysis with respect to that considered in the standard one, at least if the opening angle of the cone is not reduced to less than 0.5 rad.

8.7 Summary and combination

Table 8.1 summarises the systematic uncertainties on the measurement of M_W, both for the standard analysis and the cone analysis with several values of R.

For those uncertainties where several checks (or models) are used for the estimation,

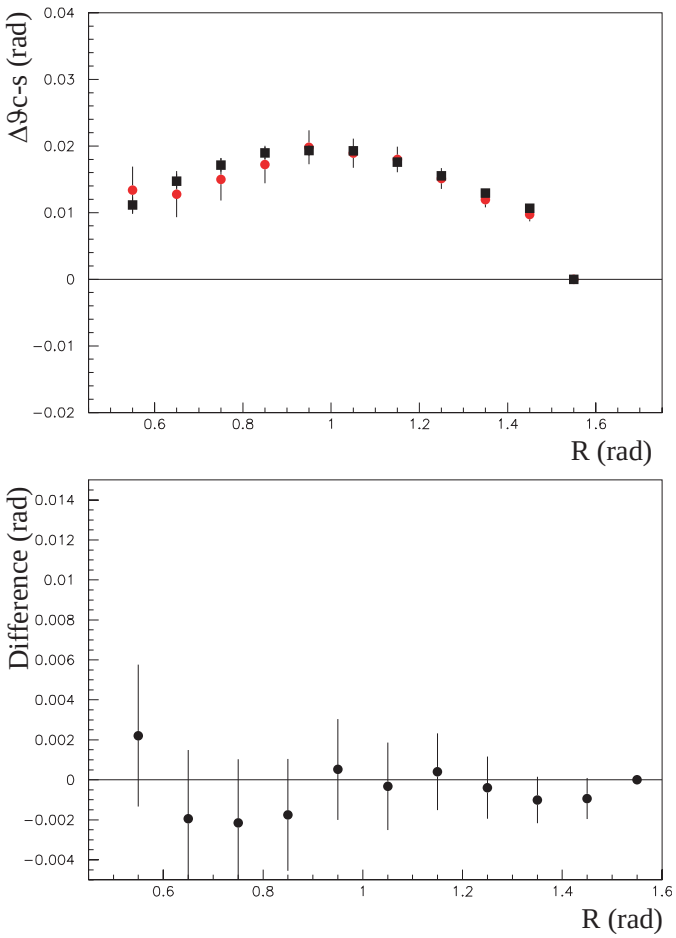

Figure 8.9: Difference between the inter-jet angles as measured using the cone and the DURHAM algorithms, for data (dots) and MC (squares). Results are shown for semileptonic events with the lepton identified as a muon. The bottom plot shows the difference between data and MC.

the maximum absolute value of ΔM_W is taken as systematic uncertainty. For the case of SK1, the bias considered is that corresponding to $\kappa_I = 2.13$. This model is giving the largest shift for analyses with R larger than 0.5 radians. For narrower cones, the largest shift comes from AR2.

For those effects for which the estimated ΔM_W depends on $\sqrt{s}$, the systematic uncertainty shown in Table 8.1 corresponds to the average obtained by weighting on the corresponding luminosities. The final contribution to the combined measurement will be slightly different, as the proper combination takes into account the systematic uncertainties at each $\sqrt{s}$, as well as the correlation matrix from the E_{beam} measurement.

	ΔM_W (MeV)			
Source	Standard	R =1.0	R =0.75	R =0.5
Theory	5			
Jet energy corrections	5			
Jet energy resolution	7			
Jet angular bias/resolution	5			
Calorimeter simulation	10			
Charged tracking	6			
LEP energy	17			
Reference MC statistics	5			
Background contamination	5			
Fragmentation	11	3	9	16
BEC	40	30	28	21
CR	115	103	80	59
Total syst. uncert.	125	111	89	69

Table 8.1: The systematic uncertainties on M_{W} measurement from the fully hadronic channel.

8.8 Systematic uncertainties for the study of CR effects

For the measurement of ΔM_{C-S}, some of the main sources of systematic uncertainty affecting the measurement of M_{W} are expected to cancel. For instance, the MC used to build the reference is exactly the same for both analysis, and therefore the systematics related to background normalisation and MC statistics vanish. Other sources like LEP energy or the theoretical description of the $\mathrm{W^+W^-}$ hard process are also expected to be negligible.

For the estimation of the rest of systematic uncertainties, the double difference between the mass biases with standard and cone analyses due to each effect are computed. Results are shown in Table 8.2. The statistical uncertainties on the differences are computed by MC sub-sampling. For those effects estimated from more than one shift, the largest in absolute value is taken, as explained above in this chapter.

Note that BEC effects are treated as a systematic uncertainty in the study of CR effects.

Table 8.3 shows the expected χ^2 , under the assumption of ΔM_{C-S}=0 at each $\sqrt{s}$,

Source	$\Delta(\Delta M_{C-S})$ (MeV)		
	R =1.0 rad	R =0.75 rad	R =0.5 rad
Calorimeter simulation	5 ± 3	-7 ± 3	10 ± 8
Charged tracking	-1 ± 2	-4 ± 2	-1 ± 2
Fragmentation	-8 ± 2	7 ± 2	14 ± 3
BEC	10 ± 3	13 ± 5	19 ± 6
Total uncertainty	14	17	26

Table 8.2: The systematic uncertainties on the measurement of ΔM_{C-S}.

when systematic uncertainties are taken into account. The χ^2 value as a function of κ_I in the `SK1` model is shown in Fig. 8.10. Even when systematic uncertainties are taken into account, the most sensitive observable to CR is the shift between the standard analysis and the cone analysis with the narrowest cone. Therefore, results will be given in next chapter for $R = 0.5$ rad (the narrowest allowed, see section 8.6).

Model	Expected χ^2, including systematics		
	$R = 1$ rad	$R = 0.75$ rad	$R = 0.5$ rad
`SK1`, $P_{reco} = 100\%$	2.6	8.9	16
`SK1`,$\kappa_I = 2.13$	0.023	0.72	1.23
`HWCR`	0.18	0.125	0.093
`GAL`	0.057	0.184	0.257
`AR2`	0.044	0.023	0.037

Table 8.3: Expected values of χ^2 taking into account systematic uncertainties in the assumption of null mass shift.

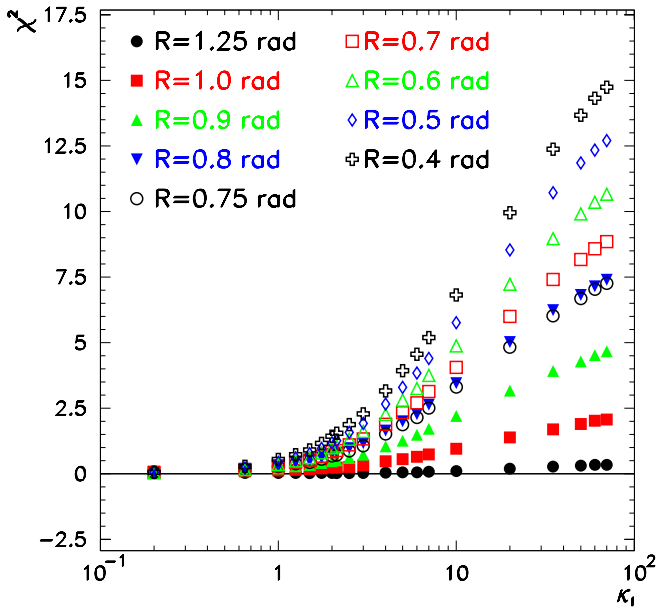

Figure 8.10: Expected values of χ^2 for ΔM_{C-S}=0, taking into account systematic uncertainties, as a function of κ_I.

Chapter 9

Results

In this chapter, the results of the analyses described in this thesis are presented. The first section gives the combined measurement of M_{W}, while results in terms of validation or exclusion of CR models are given in the second section.

9.1 Measurement of M_{W}

Table 7.3 shows the results of the mass fits for each $\sqrt{s}$, for the standard analysis and for the cone analysis with three values of R. To perform the combination of the measurements, the systematic uncertainties described in Section 8.7 are taken into account.

The value of the CR systematic has been split in the same four $\sqrt{s}$ intervals as that from E_{beam} (see Section 8.5). All the MC available at each range has been used. However, the decision on the model to be considered at each R has been taken based on the largest shift when MC at all energies is combined. As already mentioned, `SK1` with $\kappa_I = 2.13$ gives the largest shift for all the values of R considered, except for those at $R < 0.5\,\mathrm{rad}$, where `AR2` dominates.

The combined value of M_{W} using all available data between $\sqrt{s} = 183$ and 207 GeV is:

$$M_W^{standard} = 80.504 \pm 0.057(\mathrm{stat}) \pm 0.020(\mathrm{syst}) \pm 0.118(\mathrm{CR{+}BEC}) \pm 0.013(\mathrm{LEP})\ \mathrm{GeV}. \tag{9.1}$$

For the cone analysis, the mass combination has been performed for all the values

of the R parameter of the cone algorithm. The minimum total error corresponds to $R = 0.5\,\mathrm{rad}$. In this case, the measured M_{W} is:

$$M_W^{cone} = 80.473 \pm 0.067(\mathrm{stat}) \pm 0.023(\mathrm{syst}) \pm 0.054(\mathrm{CR{+}BEC}) \pm 0.013(\mathrm{LEP})\ \mathrm{GeV}. \tag{9.2}$$

The total uncertainty is reduced by the use of the cone algorithm, from 133 to 90 MeV. The relative improvement will be larger for the LEP combination, as the CR systematic uncertainty is fully correlated between experiments.

9.2 CR studies using the cone algorithm

As shown in Section 8.8, the ΔM_{C-S} analysis maximises the sensitivity to CR effects at $R = 0.5\,\mathrm{rad}$. At this R, the combination of the measurements at every $\sqrt{s}$ gives

$$\Delta M_{C-S} = -33 \pm 53(\mathrm{stat}) \pm 26(\mathrm{syst})\ \mathrm{MeV}. \tag{9.3}$$

The result of the measurement is statistically compatible with null or small CR effects on M_{W}.

Following the procedure described in previous chapters, a χ^2 is built for each CR model, from the comparison of the predicted and observed values of ΔM_{C-S} at each $\sqrt{s}$. The results are shown in Table 9.1. As expected, all those models that predict values of ΔM_{C-S} of the order of the systematic uncertainty in the measurement can not be disfavoured by the method. However, the `SK1` model with a 100% reconnection is in clear contradiction with the observed results.

The curve obtained for the κ_I scan in the `SK1` model is shown in Fig. 9.1. The minimum is found at $\kappa_I = 1.5$. By numerical integration of the corresponding likelihood function, the exclusion limit at a 68%(95%) C.L. is found to be $\kappa_I = 8.63(28.4)$. These results are in good agreement with those from the particle flow analysis at ALEPH [64] and LEP combined [65]. Note that the results are statistically compatible with the predictions of the standard unreconnected `JETSET` model.

As mentioned in Section 3.3.2, the case of $P_{reco} = 100\%$ is disfavoured by the LEP-wide particle flow analysis with $\Delta\chi^2 = 5.2$. The ΔM_{C-S} analysis using only ALEPH

Model	χ^2
Standard JETSET	4.84
Standard HERWIG	4.67
Standard ARIADNE	5.29
SK1, $P_{reco} = 100\%$	15.6
SK1,$\kappa_I = 2.13$	3.85
SK1,$\kappa_I = 1.5$	3.74
HWCR	4.08
GAL	4.29
AR2	5.02

Table 9.1: Observed values of χ^2 function for the available CR models, using ΔM_{C-S} with $R = 0.5$ rad. For the SK1 model, three options are shown: fully reconnected, with $\kappa_I = 2.13$, and that minimising χ^2: $\kappa_I = 1.5$

data disfavours it with $\Delta\chi^2 = 15.6$. In conclusion, the ΔM_{C-S} analysis disfavours more significantly large values of κ_I than the particle flow analysis.

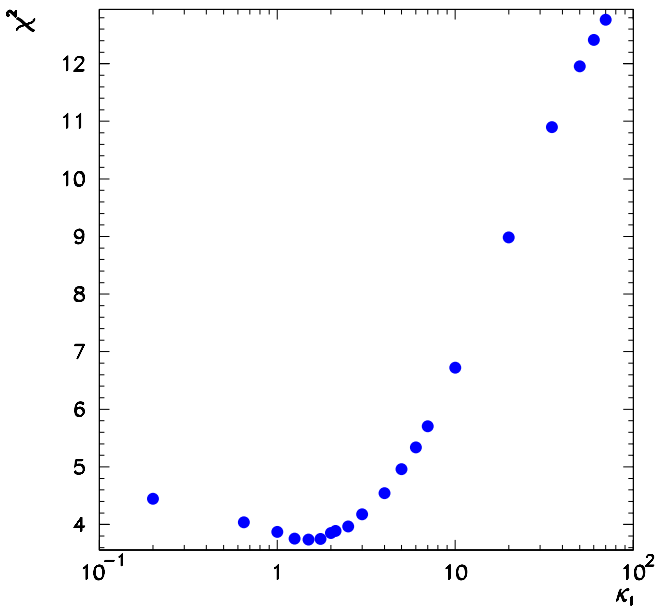

Figure 9.1: Measured χ^2 as a function of κ_I, for $R = 0.5$ rad.

Chapter 10

Summary and conclusions

The direct measurement of the W mass provides an experimental test of the Standard Model, and constraints the mass of the only particle of the model yet to be observed, the Higgs boson. In this analysis, the W mass has been measured using all the data collected by ALEPH in the fully hadronic channel above the W^+W^- production threshold. The direct reconstruction method has been used.

The measurement by direct reconstruction of the hadronic channel has some additional challenges compared to that of the semileptonic channel. There are large uncertainties on the interactions between the hadronisation cascades of the two $q\bar{q}$ systems, that affect the simulation of the MC events used as fitting reference for the measurement.

In this work, a dedicated jet algorithm has been proposed to reduce the sensitivity of the measurement to such QCD-related effects. With the use of the new cone algorithm, the total error of the mass measurement decreases. In addition, the balance of statistical and systematic uncertainties is modified, towards a largest statistical component.

The standard measurement of M_W based on the use of the `DURHAM` jet algorithm gives a result of $M_W = 80.504 \pm 133\,\text{MeV}$. The analysis based on the cone algorithm with $R = 0.5\,\text{rad}$ optimises the total error, yielding $M_W = 80.473 \pm 90\,\text{MeV}$.

The difference between the results of the W mass measurements with the standard and the cone analyses has been shown to have sensitivity to the presence of CR effects. The value measured using $R = 0.5\,\text{rad}$ is $\Delta M_{C-S} = -33 \pm 59\,\text{MeV}$. The result of the measurement is compatible with null or small CR effects on M_W.

The comparison of the observed value to those predicted by the `SK1` model has allowed to exclude a region of κ_I parameter of the model. Values of κ_I lower than 8.63(28.4) have

been excluded at a 68%(95%) C.L. The minimum in the χ^2 function lies at $\kappa_I = 1.5$, and the extreme scenario of $P_{reco} = 100\%$ is disfavoured with $\Delta\chi^2 = 15.6$.

Bibliography

[1] S.L. Glashow, Nucl. Phys. **22** (1961) 579;
S. Weinberg, Phys. Rev. Lett. **19** (1967) 1264;
A. Salam, *Elementary Particle Theory*, N. Svartholm (ed.), Almqvist and Wiksell, Stockholm (1968) 367.

[2] *Search for the Standard Model Higgs boson at LEP* ALEPH Collaboration, DELPHI Collaboration, L3 Collaboration, OPAL Collaboration, the LEP Higgs Working Group, LHWG Note/2002-01, ALEPH 2002-024. Contributed to the International Conference on High Energy Physics, Amsterdam, July 2002.

[3] S.L. Glashow, J. Iliopoulos and L. Maiani, Phys. Rev. **D2** (1970) 1285.

[4] G. 't Hooft, Nucl. Phys. **B33** (1971) 173.

[5] N. Cabbibo, Phys. Rev. Lett. **10** (1963) 531;
M. Kobayashi and K. Maskawa, Prog. Theor. Phys. **49** (1973) 652.

[6] Y. Fukuda et al., Phys. Rev. Lett. **81** (1998) 1562. S. Fukuda et al., Phys. Rev. Lett. **86** (2001) 5656. Phys. Rev. Lett. **89** 11302 (2002). Phys. Rev. Lett **89** 11301 (2002).

[7] The LEP Collaborations (ALEPH, DELPHI, L3 and OPAL), The LEP Electroweak Working Group and the SLD Heavy Flavour Group, *A combination of preliminary electroweak measurements and constraints on the Standard Model*, ALEPH 2002-011 (2002).

[8] V.S. Fadin, V.A. Khoze, A.D. Martin and A. Chapovsky, Phys. Rev. **D52** (1995) 1377.

[9] Particle Data Group, Eur. Phys. J. **C3** (1998) 19.

[10] T. Muta, R. Najima and S. Wakaizumi, Mod. Phys. Lett. **A1** (1986) 203.

[11] M. Consoli and A. Sirlin, *Physics at LEP*, J. Ellis and R. Peccei (eds.), CERN 86-02 (1986) vol.1, 63;
F. Jegerlehner, *Testing the Standard Model*, M. Cvetič and P. Langacker (eds.), Proc. of the 1990 Theor. Adv. Study Inst. (World Scientific, Singapore, 1991) 476.

[12] D. Bardin, A. Leike, T. Riemann and M. Sachwitz, Phys. Lett. **B206** (1988) 539.

[13] W. Beenakker and F.A. Berends, *Physics at LEP2*, G. Altarelli, T. Sjöstrand and F. Zwirner (eds.), CERN 96-01 (1996) vol.1, 79.

[14] M. Skrzypek, S. Jadach, W. Placzek ,Z. Wąs, Comput. Phys. Commun. **94** (1996) 216;
M. Skrzypek, S. Jadach, W. Placzek ,Z. Wąs, Comput. Phys. Commun. **140** (2001) 475.

[15] S. Jadach, W. Placzek, M. Skrzypek and B.F.L Ward, Phys. Rev. Lett. **D54** (1996) 5434.
S. Jadach et al., Phys. Lett. **B417** (1998) 326;
S. Jadach et al., Phys. Rev. **D61** (2000) 113010;
S. Jadach et al., *Precision predictions for (un)stable* W^+W^- *production at and beyond LEP2 energies*, hep-ph/0007012.

[16] S. Jadach, W. Placzek, M. Skrzypek, B.F.L. Ward, Z. Wąs, hep-ph/0109072.

[17] M. Skrzypek *et al.*, Phys. Lett. **B372** (1996) 289.

[18] E. Barberio and Z. Wąs, Comput. Phys. Commun. **79** (1994) 291.

[19] E.A. Kuraev and V.S. Fadin, Sov. J. Nucl. Phys. **41** (1985) 466.

[20] V.A. Khoze and W.J. Stirling, Phys. Lett. **B356** (1995) 373.

[21] J. Fleischer, F. Jegerlehner and M. Zralek, Z. Phys. **C42** (1989) 409;
F. Jegerlehner, *Radiative corrections: Results and Perspectives*, N. Dombey and F. Boudjema (eds.), NATO ASI Series, Plenum Press, New York (1990) 185.

[22] F. Teubert, *Precision Tests of the Electroweak Interactions at LEP/SLC*, Contributed to the XXII Physics in Collision Conference, Standford (California), June 2002.

[23] CDF Collaboration, *t Mass at CDF*, Contributed at ICHEP 98, Vancouver (Canada), July 1998;

D0 Collaboration, Phys. Rev. Lett. **84** (2000) 222;
The Top Averaging Group, for the CDF and D0 Collaborations, FERMILAB-TM-2084 (1999).

[24] LEPEWWG/MW/98-02, *LEP WW cross-sectionand W mass for '98 Summer conferences*, (1998).

[25] T. Affolder et al., CDF Collaboration, *Measurement of the W boson mass with the collider detector at Fermilab* hep-ex/0007044.

[26] F. Abe et al., CDF Collaboration, *Measurement of the W boson mass*, Phys. Rev. **D52** (1995) 4784.

[27] B. Abbott et al., D0 Collaboration, *A new measurement of the W boson mass at D0* hep-ex/9907028.

[28] , J. Alitti et al., UA2 Collaboration, *An Improved determination of the ratio of W and Z masses at the CERN anti-p p collider*, Phys. Lett. **B276** (1992) 354.

[29] ALEPH Collaboration, Eur. Phys. J. **C17** (2000) 241.

[30] Opal Collaboration, OPAL PN480, contributed to the International Europhysics Conference on High Energy Physics, Budapest, Oct 2001.

[31] S. Dawson, E. Eichten and C. Quigg, Phys. Rev. **D31** (1985) 1581.

[32] S. Moretti, K. Odagiri, P. Richardson, M.H. Seymour and B.R. Webber, hep-ph/0108264

[33] V.N. Gribov and L.N. Lipatov, Sov. J. Nucl. Phys. **15** (1972) 438;
Yu.L. Dokshitzer, Sov. J. Phys. JETP **46** (1977) 641;
G. Altarelli and G. Parisi, Nucl. Phys. **B126** (1977) 298.

[34] G. Corcella, I.G. Knowles, G. Marchesini, S. Moretti, K. Odagiri, P. Richardson, M.H. Seymour and B.R. Webber, hep-ph/0011363.

[35] I.G. Knowles adn G.D Lafferty, J. Phys., G : 23 (1997) 731.

[36] D. Amati and G. Veneziano, Phys. Lett **B83** (1979) 87;
A. Basetto, M. Ciafaloni and G. Marchesini, Nucl. Phys. **B163** (1980) 477;
G. Marchesini, L. Trentadue and G. Veneziano, Nuchl. Phys **B93** (1980) 155.

[37] H.B. Nielsen and P. Olesen, Nucl. Phys. **B61** (1973) 45.

[38] K.G. Wilson, Phys. Rev. **D10** 2445.

[39] W. Heisenberg, H. Euler, H B 1978 Niels Bohr Institute preprint NBI-HE-78-3;
J. Schwinger Phys. Rev. **82** (1951) 664;
E. Brezin, C. Itzykson, Phys. Rev. **D2** (1970) 1191;
A. Casher, H. Neuberger, Nussinov, Phys. Rev. **D20** (1979) 179.

[40] D. Amati, G. Veneziano, Phys. Lett. **B83** (1979) 87;
A. Bassetto, M. Ciafaloni, G. Marchesini, Nucl. Phys. **B 163** (1980) 477;
G. Marchesini, L. Trentadue, G. Veneziano, Nucl. Phys. **B181** (1981) 335;
Yu.L. Dokshitzer, S.I. Troyan, Leningrad Nuclear Physics Institute preprint N922 (1984);
Ya.I. Azimov, Yu.L. Doksihtzer, V.A. Khoze, S.I. Troyan, Phys. Lett. **B 165** (1985) 147.

[41] J. D'Hondt, ALEPH/99-092.

[42] ALEPH Collaboration, Z. Phys **C54** (1992) 75;
DELPHI Collaboration, Phys. Lett. **B286** (1992) 201;
OPAL Collaboration, Z. Phys. **C72** (1996) 389;
S. Haywood, Rutherford Appleton Laboratory preprint RAL-94-074 (1994).

[43] L. Lönnblad, T. Sjöstrand, Eur. Phys. J., **C2** (1998) 165.

[44] S. Jadach, K. Zalewski, CERN-TH/97-29, Acta Phys. Pol. **B28** (1997) 1461.

[45] I.V Andreev, M Plumer, R.M Weiner, *Quantum statistical approach to Bose-Einstein correlations and its experimental implications*, PRE-33702. - Moscow : Akad. Nauk Moscow. Fiz. Inst. P. N. Lebedev (1992) 61.

[46] ALEPH Collaboration, *Preliminary charged particle multiplicity in* $e^+e^- \to W^+W^-$, Contributed to the International Conference on High Energy Physics, Amsterdam, July 2002.

[47] L. Lönnblad, T. Sjöstrand, Phys. Lett. **B** 351 (1995) 293.

[48] K. Fialkowski, R. Wit, HEP-PH/9810492.

[49] B. Andersson, M. Ringnér, LU TP 97-07.

[50] ALEPH Collaboration, Phys. Lett., **B478** (2000) 1-3 50.

[51] ALEPH Collaboration, *Update on Bose-Einstein correlations in W-pair decays*, ALEPH note ALEPH 2000-024 CONF 2000-020, contributed to the 2000 winter conferences.

[52] ALEPH Collaboration, *Further studies on Bose-Einstein correlations in W-pair decays* ALEPH note ALEPH 2000-039 CONF 2000-059, contributed to the ICHEP, Osaka, 2000.

[53] S.V. Chekanov, E.A. De Wolf and W. Kittel, *Bose-Einstein correlations and color reconnection in W-pair production*, Eur. Phys. J. C6 (1999) 403.

[54] The LEP Collaborations (ALEPH, DELPHI, L3 and OPAL), The LEP W Working Group, *Combination of the measurements of inter-W particle correlations in* $e^+e^- \rightarrow W^+W^-$ *events at lep* Contributed to the International Conference on High Energy Physics, Amsterdam, July 2002.

[55] CLEO Collaboration, P. Haas et al., Phys. Lett. **55** (1985) 1248;
ARGUS Collaboration, H. Albrecht et al., Phys. Lett. **B162** (1985) 395. H. Fritzsch, Phys. lett **B86** (1979) 164;
J.H. Kühn, S. Nussinov, R. Rückl, Z. Phys. **C5** (1980) 117.

[56] T. Sjöstrand, V. Khoze, Z. Phys. **C62** (1994) 281.

[57] J. Ellis, K. Geiger, Phys. Rev., **D54** (1996) 1967.

[58] Z. Si,Q. Wang,Q. Xie, HEP-PH/9704226.

[59] H. Parks, Superconductivity (Marcel Dekker, New York, 1969).

[60] J. Rathsman, Phys. Let. **B452** (1999) 364.

[61] L. Lonnblad, Z. Phys. **C70** (1996) 107.

[62] L3 Collaboration,LAPP-EXP 2000-02, Presented at Workshop on WW Physics at LEP200, Kolymbari, Chania, Greece, Oct 1999.

[63] ALEPH Collaboration, ALEPH 2001-047, contributed to the International Europhysics Conference on High Energy Physics, Budapest, Oct 2001.

[64] ALEPH Collaboration, ALEPH 2002-020, contributed to the International Conference on High Energy Physics, Amsterdam, July 2002.

[65] The LEP Collaborations (ALEPH, DELPHI, L3 and OPAL), *Combined preliminary results on colour reconnection using particle flow in* $e^+e^- \rightarrow W^+W^-$, The LEP W Working Group, Contributed to the International Conference on High Energy Physics, Amsterdam, July 2002.

[66] K. Hornik, M. Stinchcombe and H. White, *Neural Networks* **2** (1989) 359;
J.A. Hertz, A. Krogh and R.G. Palmer, *Introduction to the theory of neural computation*, Addison-Wesley, Redwood City CA (1991);
B. Müller and J. Reinhardt, *Neural networks: an introduction*, Springer-Verlag, Berlin (1991).

[67] Y. Le Cun, Proc. Cognitiva **85** (1985) 599.

[68] V. Gaitan, *Neural Networks in High Energy Physics: From Pattern Recognition to Exploratory Data Analysis*, Ph.D. thesis, Universitat Autònoma de Barcelona, Barcelona (1993).

[69] V. Breton *et al.*, Nucl. Inst. and Meth. **A362** (1995) 478.

[70] The LHC Study Group, CERN/AC/95-05.

[71] D. Decamp *et al.*, ALEPH Collaboration, Nucl. Inst. and Meth. **A294** (1990) 121.

[72] P. Aarnio *et al.*, DELPHI Collaboration, Nucl. Inst. and Meth. **A303** (1991) 233.

[73] B. Adeva *et al.*, L3 Collaboration, Nucl. Inst. and Meth. **A289** (1990) 33.

[74] K. Ahmet *et al.*, OPAL Collaboration, Nucl. Inst. and Meth. **A305** (1991) 275.

[75] LEP Design Report, vol.1: *The LEP Injector Chain*, CERN-LEP/83-29 (1983);
LEP Design Report, vol.2: *The LEP Design Report*, CERN-LEP/84-01 (1984).

[76] E. Torrence, presentation at the LEP Jamboree, CERN, April 2001.

[77] LEP Energy Working Group, LEPEWG 01/01, March 2001.

[78] LEP Energy Working Group, *Calibration of centre-of-massenergies at LEP1 for precise measurements of Z properties*, CERN-EP/98-040, CERN-SL/98-012, submitted to Eur. Phys. J.

[79] A.A. Sokolov and I.M. Ternov, Sov. Phys. Dokl. **8** (1964) 1203.

[80] J. Billan *et al.*, *Determination of the Particle Momentum in LEP from Precise Magnet Measurements*, Proc. of the 1991 Particle Accelerators Conference, San Francisco, USA, May 1991.

[81] ALEPH Collaboration *Determination of the LEP centre-of-mass energy from $Z\gamma$ events*, Phys. Lett. **B464** (1999) 339;
DELPHI Collaboration, L3 Collaboration, OPAL Collaboration, *LEP2 beam energy measurement using radiative return events*, Contributed to the International Conference on High Energy Physics, Amsterdam, July 2002.

[82] ALEPH Collaboration, *The ALEPH Handbook*, C. Bowdery (ed.), vol.1 (1995); vol.2 (1997). Published by CERN.

[83] D. Buskulic *et al.*, ALEPH Collaboration, Nucl. Inst. and Meth. **A360** (1995) 481.

[84] S. Jadach, W. Placzek, E. Richter-Wąs, B.F.L. Ward and Z. Wąs, Comput. Phys. Commun. **102** (1997) 229.

[85] P. Mató, *Data processing for Large* e^+e^- *Experiments*, Ph.D. thesis, Universitat de Barcelona, Barcelona (1990).

[86] M. Delfino *et al.*, Comput. Phys. Commun. **57** (1989) 401.

[87] J. Knobloch, *JULIA Users and Programmers guide*, ALEPH internal report, ALEPH 90-11 (1990).

[88] H. Albrecht, E. Blucher and J. Boucrot, *ALPHA: Aleph Physics Analysis Package*, ALEPH internal report, ALEPH 97-058 (1997).

[89] D. Casper, *The ALEPH Tracking Upgrade. Part 1: VDET Global Pattern Recognition, Technical Documentation*, ALEPH internal report, SOFTWR 97-004 (1997).

[90] R. Frühwirth, HEPHY-PUB 503/87 (1987).

[91] B. Bloch-Devaux *et al.*, *KINGAL Users Guide*, ALEPH internal report, ALEPH 87-53 (1988).

[92] R. Brun *et al.*, *GEANT3 Users Guide*, CERN-DD/EE/84-1 (1987).

[93] F. Ranjard, *GALEPH-Monte Carloprogram for ALEPH*, ALEPH internal report, ALEPH 88-119 (1988).

[94] H. Fesefeldt, *GHEISHA*, Aachen 3rd Inst. Nucl. Phys. **A23** (Proc. Suppl.) (1991) 291.

[95] J. Fujimoto *et al.*, MINAMI-TATEYA Collaboration, *GRACE User's manual, version 2.0*, KEK report 92-19 (1993) (submitted to Comput. Phys. Commun.).

[96] T. Sjöstrand, Comput. Phys. Commun. **82** (1994) 74.

[97] F.A. Berends, G. Burgers and W.L. Van Neerven, Phys. Lett. **B185** (1987) 395; Nucl. Phys. **B297** (1988) 429; Nucl. Phys. **B304** (1988) 921.

[98] D. Buskulic *et al.*, ALEPH Collaboration, Phys. Lett. **B313** (1993) 509.

[99] S. Jadach, B.F.L. Ward and Z. Wąs, Comput. Phys. Commun. **79** (1994) 466.

[100] H. Anlauf *et al.*, Comput. Phys. Commun. **79** (1994) 466.

[101] I. Riu, *Measurement of the W mass from the* $W^+W^- \to q\bar{q}q\bar{q}$ *channel with the ALEPH detector*, Ph.D. thesis, Universitat Autonoma de Barcelona, 1998.

[102] M. Chalmers *Measurements of the mass of the W boson in the* $W^+W^- \to q\bar{q}q\bar{q}$ *channel with the ALEPH detector*, Ph.D. thesis, University of Glasgow, 1999.

[103] ALEPH Collaboration, *Measurement of the W-pair cross-section in ee collisions at 172 GeV* Phys. Lett. **B415** (1997) 435

[104] J. Nowell, *A measurement of the W Boson mass with the ALEPH detector*, Ph.D. thesis, Imperial College, 1999.

[105] `http://alephwww.cern.ch/~hansenjo/ALEPH-ONLY/abcfit/abcfit.html`

[106] ALEPH Collaboration *Measurement of the W-pair cross-section in ee collisions at 189 GeV* Phys. Lett. **B487** (2000) 241.

[107] ALEPH Collaboration *Measurement of W-pair production and W branching ratios in* e^+e^- *collisions up to 208 GeV*, ALEPH 2001-013 CONF (CONFerence) 2001-010.

[108] A. Juste, M. Martinez, F. Teubert, *On calibration curves* ALEPH 97-048 PHYSICS 97-042.

[109] ALEPH Collaboration, *Measurement of the W mass by direct reconstruction in e+ e- collisions at 172-GeV*, Phys. Lett. **B422** (1998) 384.

[110] D. Bardin et al., *GENTLE/4fan v. 2.0: A program for the semi-analytic calculation of predictions for the process* $e^+e^- \to 4f$, Comput. Phys. Commun **104** (1997) 161.

[111] F. James, M. Roos, *'MINUIT', a System for Function Minimization and Analysis of the Parameter Errors and Correlations*, Comput. Phys. Commun. **10** (1975) 343.

[112] K. Fialkowski, R. Wit, hep-ph/9709205, Acta Phys. Pol. **B28** (1997) 2039;
V. Kartvelishvili, R. Kvatadze, R. Moller, Phys. Lett. **B408** (1997) 331.

[113] J. Hakkinen, M. Ringner, Eur. Phys. J. **C5** (1998) 275;
S. Todorova-Nova, J. Rames, hep-ph/9710280, PRA-HEP 97/16.

[114] *Run II Jet Physics*, Proceedings of the Run II QCD and Weak Boson Physics Workshop, hep-ex/0005012.

[115] M. Skrzypek, S. Jadach, W. Placzek and Z. Wąs, Comput. Phys. Commun. **94** (1996) 216;
M. Skrzypek et al., Phys. Lett. **B372** (1996) 289;
S. Jadach et al., Comput. Phys. Commun. **119** (1999) 272.

[116] A. Denner, S. Dittmaier, M. Roth and D. Wackeroth, Nucl. Phys. **B587** (2000) 67;
A. Denner, S. Dittmaier, M. Roth and D. Wackeroth, Nucl. Phys. Proc. Supl. **89** (2000) 100.

[117] I. Riu *W Mass Background Systematic Study using Z peak data*, ALEPH 97-060.

[118]
`http://venturi.home.cern.ch/venturi/ALEPH/WW/systematics/detector_test.html`